

# MJO—skeleton and conceptual models

To appear in: Encyclopedia of Atmospheric Science, 2nd Edition  
October 18, 2012

**Andrew J. Majda**

Courant Institute of Mathematical Sciences, New York University

**Samuel N. Stechmann**

University of Wisconsin-Madison

## Abstract

The Madden–Julian Oscillation’s (MJO’s) “skeleton” is its fundamental features on intraseasonal/planetary scales: (i) slow eastward phase speed of roughly 5 m/s, (ii) peculiar dispersion relation with  $d\omega/dk \approx 0$ , and (iii), horizontal quadrupole vortex structure. The MJO skeleton model is a minimal, nonlinear oscillator model that captures these three features together. The fundamental mechanism involves interactions between moisture, convective activity, and equatorial fluid dynamics. Further details beyond the MJO skeleton are referred to as the MJO’s “muscle” and include refined vertical structure and upscale convective momentum transport from sub-planetary-scale convection and waves.

## 1 Introduction

The Madden-Julian Oscillation (MJO) is the dominant component of intraseasonal ( $\approx 30$ -60 days) variability in the tropics. This variability appears not only in the wind, pressure, and temperature fields, but also in water vapor and convection. The structure of the MJO is a planetary-scale ( $\approx 10,000$ -40,000 km) circulation cell with regions of enhanced and suppressed convection, and it propagates slowly eastward at a speed of roughly 5 m/s. The main regions of MJO activity are the Indian and western Pacific Oceans, and the MJO interacts with monsoons, tropical cyclones, ENSO, and other tropical phenomena. Nevertheless, while the MJO is mainly a tropical phenomenon, it also interacts with the extratropics and can affect midlatitude predictability.

The fundamental features of the MJO on intraseasonal–planetary scales are referred to here as the MJO’s “skeleton”:

- I. Slow eastward phase speed of roughly 5 m/s,
- II. Peculiar dispersion relation with  $d\omega/dk \approx 0$ , and
- III. Horizontal quadrupole–vortex structure.

While these are the salient planetary–intraseasonal features of MJO composites, individual MJO events often have additional features, such as westerly wind bursts, and different varieties of convective features within the MJO envelope. Since these additional features add detailed character to each MJO’s structure, and since these features often account for additional strength beyond the MJO’s skeleton, they are referred to here as the MJO’s “muscle.”

While the MJO is often described as an intraseasonal–planetary scale phenomenon, it actually has a complex multiscale structure. The MJO’s region of enhanced convection is composed of a menagerie of smaller-scale convective processes, including synoptic-scale convectively coupled equatorial waves (CCEWs), mesoscale convective systems (MCSs), and tropical cyclones. Hence the MJO is essentially an envelope of sub-planetary-scale convective activity and is a multiscale phenomenon. In light of this, multiscale interactions are a key part of the theory for the MJO’s skeleton and muscle.

The MJO skeleton model is a minimal dynamical model that captures the MJO’s intraseasonal–planetary scale features I-III together. The model is a nonlinear oscillator model whose fundamental mechanism involves interactions between moisture, convective activity, and equatorial fluid dynamics. Before presenting the full MJO skeleton model, these main components are described individually.

## 2 Dry Equatorial Long-wave Equations

The equatorial long-wave equations describe equatorial dynamics on planetary spatial scales of  $O(10,000 \text{ km})$  in the zonal  $x$  direction and intraseasonal time scales of  $O(10 \text{ days})$  or longer. The equations take the form

$$\frac{\partial u'}{\partial t} - yv' + \frac{\partial p'}{\partial x} = 0 \quad [1]$$

$$yu' + \frac{\partial p'}{\partial y} = 0 \quad [2]$$

$$\frac{\partial p'}{\partial z} = \theta' \quad [3]$$

$$\frac{\partial u'}{\partial x} + \frac{\partial v'}{\partial y} + \frac{\partial w'}{\partial z} = 0 \quad [4]$$

$$\frac{\partial \theta'}{\partial t} + w' = 0 \quad [5]$$

Here  $u'$ ,  $v'$ , and  $w'$  are the zonal, meridional, and vertical velocity anomalies, respectively; and  $p'$  and  $\theta'$  are the pressure and potential temperature anomalies, respectively. Notice that the  $\partial v'/\partial t$  term is small in this long-wave limit, and hence geostrophic balance is satisfied in the meridional  $y$  direction but not the zonal  $x$  direction. The Coriolis terms  $-yv'$  and  $yu'$  vanish at the equator ( $y = 0$ ) and are written using the equatorial beta-plane approximation. The equations [1]–[5] have been nondimensionalized using the standard equatorial reference scales described in Table 1.

[TABLE 1 ABOUT HERE]

The wave solutions of [1]–[5] can be found by expanding in vertical and meridional basis functions. First, each variable is expanded in terms of vertical structure functions such as  $u'(x, y, z, t) = \sum_j u'_j(x, y, t)\sqrt{2}\cos(jz)$ , etc. This allows the equations [1]–[5] to be separated into an infinite number of (long-wave) shallow water systems, where each mode  $j$  corresponds to a separate independent

Table 1: Constants and reference scales for nondimensionalization.

Parameter	Derivation	Value	Description
$\beta$		$2.3 \times 10^{-11} \text{ m}^{-1} \text{ s}^{-1}$	Variation of Coriolis parameter with latitude
$\theta_0$		300 K	Potential temperature at surface
$g$		$9.8 \text{ m s}^{-2}$	Gravitational acceleration
$H$		16 km	Tropopause height
$N^2$	$(g/\theta_0)d\bar{\theta}/dz$	$10^{-4} \text{ s}^{-2}$	Buoyancy frequency squared
$c$	$NH/\pi$	$50 \text{ m s}^{-1}$	Velocity scale
$L$	$\sqrt{c/\beta}$	1500 km	Equatorial length scale
$T$	$L/c$	8 hrs	Equatorial time scale
	$HN^2\theta_0/(\pi g)$	15 K	Potential temperature scale
	$H/\pi$	5 km	Vertical length scale
	$H/(\pi T)$	$0.2 \text{ m s}^{-1}$	Vertical velocity scale
	$c^2$	$2500 \text{ m}^2 \text{ s}^{-2}$	Pressure scale

(long-wave) shallow water system. For the first baroclinic mode,  $j = 1$ , the system has the form

$$\frac{\partial u'}{\partial t} - yv' - \frac{\partial \theta'}{\partial x} = 0 \quad [6]$$

$$yu' - \frac{\partial \theta'}{\partial y} = 0 \quad [7]$$

$$\frac{\partial \theta'}{\partial t} - \frac{\partial u'}{\partial x} - \frac{\partial v'}{\partial y} = 0 \quad [8]$$

where the subscript  $j = 1$  has been dropped from all variables.

Next, through meridional expansion, this long-wave shallow water system can be separated into equations for an infinite set of zonally propagating, equatorially trapped waves. This is achieved by expanding the variables  $u', v', \theta'$  in terms of meridional basis functions such as  $u'(x, y, t) = \sum_m u'_m(x, t)\phi_m(y)$  etc. Here the appropriate meridional basis functions are the parabolic cylinder functions, the first few of which are  $\phi_0(y) = \pi^{-1/4} \exp(-y^2/2)$ ,  $\phi_1(y) = \pi^{-1/4} \sqrt{2}y \exp(-y^2/2)$ , and  $\phi_2(y) = \pi^{-1/4} 2^{-1/2}(2y^2 - 1) \exp(-y^2/2)$ . Notice the  $\exp(-y^2/2)$  factor in each of the parabolic cylinder functions, whose rapid decay away from the equator,  $y = 0$ , corresponds to the terminology “equatorially trapped waves”. Through such a meridional expansion, one can derive the infinite set of equations

$$\frac{\partial K'}{\partial t} + \frac{\partial K'}{\partial x} = 0 \quad [9]$$

$$\frac{\partial R'_1}{\partial t} - \frac{1}{3} \frac{\partial R'_1}{\partial x} = 0 \quad [10]$$

$$\frac{\partial R'_2}{\partial t} - \frac{1}{5} \frac{\partial R'_2}{\partial x} = 0 \quad [11]$$

$$\frac{\partial R'_3}{\partial t} - \frac{1}{7} \frac{\partial R'_3}{\partial x} = 0 \quad [12]$$

⋮

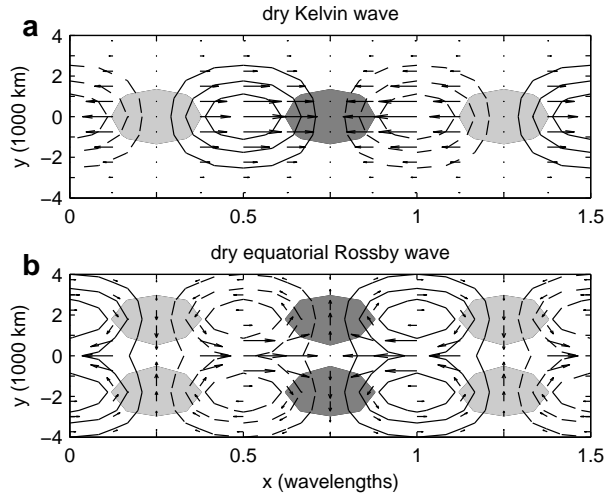


Figure 1: Horizontal structures of two unforced “dry” equatorial long-waves: (a) Kelvin wave, and (b) the first equatorial Rossby wave,  $R'_1$ . Contours show lower tropospheric pressure with positive (negative) anomalies denoted by solid (dashed) lines. The contour interval is one-fourth the maximum amplitude of the anomaly, and the zero contour is not shown. Anomalies of convergence (divergence) that are greater than two-thirds the maximum amplitude are shaded dark (light) gray. From Majda and Stechmann (2009) *Proceedings of the National Academy of Sciences USA*.

Here  $K, R_1, R_2, R_3, \dots$  are the amplitudes of equatorial long-wave Kelvin and Rossby waves, respectively. The variables  $u'(x, y, t), v'(x, y, t), \theta'(x, y, t)$  are recovered using the relationships between the primitive variables  $u'_m(x, t), v'_m(x, t), \theta'_m(x, t)$  and the wave amplitudes  $K'(x, t), R'_m(x, t)$ . For instance,  $u'_0(x, t) = [K'(x, t) - R'_1(x, t)/2]/\sqrt{2}$ , etc. To illustrate this, Figure 1 shows  $u', v', \theta'$  for the two separate cases with either  $K'(x) = -\cos(x)$  or  $R'_1(x) = \cos(x)$ . These illustrations can be thought of as the meridional structures associated with the wave amplitudes  $K'(x, t)$  and  $R'_1(x, t)$ .

[FIGURE 1 ABOUT HERE]

The dispersion relations for the waves from [9]–[12] are seen to be  $\omega_K(k) = k$ ,  $\omega_{R1}(k) = k/3$ ,  $\omega_{R2}(k) = k/5$ , etc., which arise from assuming solutions of the form  $K'(x, t) = \exp(i[kx - \omega_K(k)t])$ , etc. Hence these waves are non-dispersive in this long-wave limit.

### 3 Moisture-Convection Interactions on Intraseasonal–Planetary Scales

Besides the fluid dynamical core, the second main component of the MJO skeleton model is moisture–convection interactions. These quantities are represented by the variables  $q'$  and  $a$ , respectively:

- $q'$  : lower tropospheric moisture anomaly,
- $a$  : amplitude of the convection/wave activity envelope.

It is noteworthy that, for the MJO skeleton model, it is only the amplitude of the convection/wave activity envelope that is needed, not any of the details of the particular convection/waves that make up the envelope, although the specific details can be important for convective momentum transports or other features of the MJO’s “muscle”. Also notice that  $a$ , without a prime, is not an anomaly.

A key part of the  $q$ -and- $a$  interaction is how the moisture anomalies influence the convection. The premise is that, for convective activity on planetary–intraseasonal scales, it is the *time tendency* of convective activity – not the convective activity itself – that is most directly related to the (lower-tropospheric) moisture anomaly. In other words, rather than a functional relationship  $a = a(q)$ , it is posited that  $q$  mainly influences the tendency – i.e., the growth and decay rates – of the convective activity. The simplest equation that embodies this idea is

$$\frac{\partial a}{\partial t} = \Gamma q' a, \tag{13}$$

where  $\Gamma$  is a constant of proportionality: positive low-level moisture anomalies create a tendency to enhance the envelope of convection/wave activity, and negative low-level moisture anomalies create a tendency to decrease the envelope of convection/wave activity.

The basis for [13], and the physics behind it, comes from a combination of observations, modeling, and theory. Generally speaking, it is well-known that tropospheric moisture content plays a key role in regulating convection. On planetary–intraseasonal scales specifically, several studies have shown that the lower troposphere tends to moisten during the suppressed convection phase of the MJO, and lower tropospheric moisture leads the MJO’s heating anomaly, which suggests the relationship [13]. Furthermore, this relationship is also suggested by simplified models for synoptic-scale convectively coupled waves, which show that the growth rates of the convectively coupled waves depend on the wave’s environment, such as the environmental moisture content. In [13], the factor  $\Gamma q'$  acts as a growth/decay rate for the convective activity, and the value of  $\Gamma$  has been estimated from these growth rate variations in idealized models of convectively coupled waves. Lastly, amplitude equations such as [13] have been used in other areas of science and engineering, and they can sometimes be derived from the governing equations using systematic asymptotics.

## 4 MJO Skeleton Model

By combining the parameterization [13] with the (long-wave scaled) linearized primitive equations [1]–[5], the MJO skeleton model is obtained:

$$\frac{\partial u'}{\partial t} - yv' + \frac{\partial p'}{\partial x} = 0 \quad [14]$$

$$yu' + \frac{\partial p'}{\partial y} = 0 \quad [15]$$

$$\frac{\partial p'}{\partial z} = \theta' \quad [16]$$

$$\frac{\partial u'}{\partial x} + \frac{\partial v'}{\partial y} + \frac{\partial w'}{\partial z} = 0 \quad [17]$$

$$\frac{\partial \theta'}{\partial t} + w' = \bar{H}a - s^\theta \quad [18]$$

$$\frac{\partial q'}{\partial t} - \tilde{Q}w' = -\bar{H}a + s^q \quad [19]$$

$$\frac{\partial a}{\partial t} = \Gamma q'a. \quad [20]$$

An equation for the lower-tropospheric moisture  $q'$  is also included in the system in [19]. The terms  $\pm \bar{H}a$  represent a heat source and moisture sink due to convective activity, and  $s^\theta$  and  $s^q$  represent radiative cooling and a moisture source, respectively.

Notice that this model contains a minimal number of parameters:  $\tilde{Q} = 0.9$ , the (nondimensional) mean background vertical moisture gradient; and  $\Gamma = 1$ , or  $\Gamma \approx 0.2 \text{ K}^{-1} \text{ d}^{-1}$  in dimensional units. The source terms  $s^\theta$  and  $s^q$  must also be specified (see below). Also notice that the parameter  $\bar{H}$  is actually irrelevant to the dynamics (as can be seen by rescaling  $a$ ); it is written here for clarity of presentation: dimensionally, it gives  $\bar{H}a$  the units of a heating rate while keeping  $a$  nondimensional. The dimensional value of  $\bar{H}$  was chosen to be 10 K/day so that a typical value of  $a$  is  $\approx 0.1$ , similar to the nondimensional value of  $u$ .

The MJO skeleton model [14]–[20] is a *nonlinear oscillator* model for the MJO skeleton as a neutrally stable wave. In other words, the model includes neither damping nor instability mechanisms. The fundamental mechanism of the oscillation involves interactions between moisture, convection, and circulation. The nonlinear oscillator component can be seen in the terms  $\partial q'/\partial t = -\bar{H}a$  and  $\partial a/\partial t = \Gamma q'a$ . However, there is also the important moisture convergence term,  $\tilde{Q}w'$ , which couples this  $q$ -and- $a$  oscillator to the circulation.

To obtain the simplest model for the MJO, truncated vertical and meridional structures are used. The procedure is analogous to the case of the dry equatorial long-wave equations described above, where equations for the *dry* zonally propagating, equatorially trapped waves  $K'(x, t)$ ,  $R'_j(x, t)$  were derived. For the vertical truncation, only the first baroclinic mode is used in the simplest model so

that  $u'(x, y, z, t) = u'(x, y, t)\sqrt{2}\cos(z)$ , etc. The resulting equations are

$$\frac{\partial u'}{\partial t} - yv' - \frac{\partial \theta'}{\partial x} = 0 \quad [21]$$

$$yu' - \frac{\partial \theta'}{\partial y} = 0 \quad [22]$$

$$\frac{\partial \theta'}{\partial t} - \frac{\partial u'}{\partial x} - \frac{\partial v'}{\partial y} = \bar{H}a - s^\theta \quad [23]$$

$$\frac{\partial q'}{\partial t} + \tilde{Q} \left( \frac{\partial u'}{\partial x} + \frac{\partial v'}{\partial y} \right) = -\bar{H}a + s^q \quad [24]$$

$$\frac{\partial a}{\partial t} = \Gamma q' a. \quad [25]$$

Next, for the meridional truncation, the variables are expanded in terms of the parabolic cylinder functions  $\phi_m(y)$  as described above for the *dry* equatorial long-wave equations. It is also assumed that  $q$  and  $a$  have simple equatorial meridional structure proportional to  $\exp(-y^2/2)$ :  $a(x, y, t) = [\bar{A}(x) + A'(x, t)]\phi_0(y)$ , where  $\bar{A}(x)$  is a background state. For the long-wave-scaled equations, such a meridional heating structure is known to couple with only Kelvin waves and the first symmetric equatorial Rossby waves  $R'_1$ , and the resulting meridionally truncated equations can be written as

$$\frac{\partial K'}{\partial t} + \frac{\partial K'}{\partial x} = -\frac{1}{\sqrt{2}}\bar{H}A' \quad [26]$$

$$\frac{\partial R'}{\partial t} - \frac{1}{3}\frac{\partial R'}{\partial x} = -\frac{2\sqrt{2}}{3}\bar{H}A' \quad [27]$$

$$\frac{\partial Q'}{\partial t} + \frac{1}{\sqrt{2}}\tilde{Q}\frac{\partial K'}{\partial x} - \frac{1}{6\sqrt{2}}\tilde{Q}\frac{\partial R'}{\partial x} = \left(-1 + \frac{1}{6}\tilde{Q}\right)\bar{H}A' \quad [28]$$

$$\frac{\partial A'}{\partial t} = \Gamma Q'(\bar{A} + A'), \quad [29]$$

where the subscript 1 has been dropped from  $R'_1$  for brevity. The equations have been written in terms of anomalies from the state of radiative–convective equilibrium,  $\bar{H}\bar{A}(x) = S^\theta(x) = S^q(x)$ . Two simple cases are a uniform background state with constant  $\bar{S}^\theta = 1$  K/day and a spatially varying state  $S^\theta(x)$  that represents a warm-pool sea surface temperature distribution.

An important point is that  $K'(x, t)$  and  $R'(x, t)$  are the amplitudes of the *structures* of Kelvin and Rossby waves, but these amplitudes in [26]–[27] need not always *propagate* like “dry” waves. In the absence of forcing in [9]–[10], the “dry” long-wave Kelvin and equatorial Rossby wave solutions are dispersionless waves that propagate at 50 and 17 m/s, respectively. However, in the presence of the coupled dynamical forcing  $A$  in [26]–[29], the Kelvin and equatorial Rossby wave *structures* can be coupled to each other and to  $Q$  and  $A$ ; and these coupled modes/structures can have propagation speeds very different from 50 or 17 m/s, and they can be dispersive. One such mode has a mixed Kelvin–Rossby wave structure and dispersion characteristics of the MJO and is summarized below.

#### 4.1 Energetics

The nonlinear MJO skeleton model has two important energy principles, in the absence of source terms  $s^\theta$  and  $s^q$ . First, the model [21]–[25] conserves a vertically integrated moist static energy:

$$\partial_t(\theta + q) - (1 - \tilde{Q})(u_x + v_y) = 0. \quad [30]$$

Second, this model conserves a positive total energy that includes a contribution from the convective activity  $a$ :

$$\partial_t \left[ \frac{1}{2}u^2 + \frac{1}{2}\theta^2 + \frac{1}{2} \frac{\tilde{Q}}{1-\tilde{Q}} \left( \theta + \frac{q}{\tilde{Q}} \right)^2 + \frac{\bar{H}}{\Gamma\tilde{Q}}a \right] - \partial_x(u\theta) - \partial_y(v\theta) = 0. \quad [31]$$

This total energy is a sum of four terms: dry kinetic energy  $u^2/2$ , dry potential energy  $\theta^2/2$ , a moist potential energy proportional to  $(\theta + \tilde{Q}^{-1}q)^2$ , and a convective energy  $\bar{H}a/(\Gamma\tilde{Q})$ . Note that the natural requirement on the background moisture gradient,  $0 < \tilde{Q} < 1$ , is needed to guarantee a positive energy.

## 4.2 Linear theory results

Now the linear modes of the model are presented. Since the model [26]–[29] involves four dynamically coupled variables, there are four linear modes. The dispersion relation for the linear modes is shown in Figure 2. (Only the two low-frequency, intraseasonal modes are shown. The other two modes are high-frequency modes and are only weakly coupled to the wave activity.) Figure 2 shows that the skeleton model has eastward-propagating waves with phase speeds of roughly 5 m/s and the peculiar dispersion relation  $d\omega/dk \approx 0$ , in agreement with the MJO. Moreover, the phase speed and dispersion relation are robust over a wide range of parameter values, with the oscillation periods spanning the range of 30–60 days, which is the observed range of the MJO’s oscillation period. The westward-propagating waves, on the other hand, which are plotted with positive  $\omega$  and negative  $k$ , have frequencies  $\omega(k)$  that vary significantly with  $k$ ; moreover, their oscillation periods are seasonal, not intraseasonal, for  $k = 1$  and 2. This suggests the first piece of an explanation for the observed dominance of eastward-propagating intraseasonal variability: the westward-propagating modes have seasonal oscillation periods, on which time scales other phenomena are expected to dominate over modulations of convective activity.

[FIGURE 2 ABOUT HERE]

The features in Figure 2 are fundamental features I–II of the MJO skeleton that were mentioned in the Introduction section. For a linear wave, these two features arise from the eigenvalues of the linear system. The second important piece from the linear system is the eigenvectors, which determine the structure of the linear waves and fundamental feature III from the Introduction section. When trying to match theory and observations, it is important that both the eigenvalues and eigenvectors—i.e., all three fundamental features I–III—are matched together.

The physical structure of the wavenumber-2 MJO eigenmode is shown in Figure 3 for the standard parameter values. Horizontal quadrupole vortices are prominent, as in observations, and the maximum convective activity is colocated with the maximum in equatorial convergence. The lower tropospheric moisture leads and is in quadrature with the convective activity, which is also roughly the relationship seen in observations. The pressure contours display the mixed Kelvin/Rossby wave structure of the wave: equatorial high pressure anomalies are colocated with the westerly wind burst as in Kelvin waves, and they are flanked by off-equatorial low pressure anomalies and cyclonic Rossby gyres, in broad agreement with the observational record. Rectification of the vertical structure and some of the phase relationships is likely due to effects of higher vertical modes as part of the MJO’s “muscle”.

[FIGURE 3 ABOUT HERE]

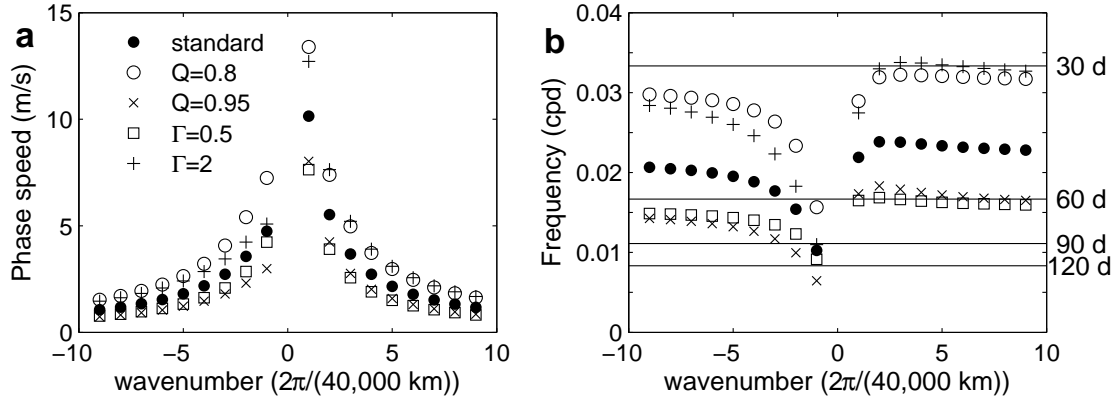


Figure 2: Linear wave phase speed  $\omega/k$  (a) and oscillation frequency  $\omega(k)$  (b) as functions of wavenumber  $k$  for the low-frequency modes of [26]–[29]. Filled circles denote results with the standard parameter values. Other markers denote results with one change made to the standard parameter values:  $\tilde{Q} = 0.8$  (open circles),  $\tilde{Q} = 0.95$  (crosses),  $\Gamma = 0.5$  (squares), and  $\Gamma = 2$  (pluses). Horizontal lines in (b) denote oscillation periods of 30, 60, 90, and 120 days. From Majda and Stechmann (2009) *Proceedings of the National Academy of Sciences USA*.

The relative contributions of  $K, R, Q$ , and  $A$  to these linear waves are shown in Fig. 4 for wavenumbers 1, 2, and 3. The MJO has significant contributions from both the Kelvin and Rossby components, whereas the westward modes are dominated by the Rossby component. In addition, the larger  $Q$  and  $A$  amplitudes suggest the second piece of an explanation for eastward-propagating rather than westward-propagating intraseasonal oscillations: the eastward-propagating modes are more strongly coupled to equatorial moist convective processes.

[FIGURE 4 ABOUT HERE]

In addition to these illustrations, a formula for the intraseasonal oscillation frequency  $\omega$  of the MJO skeleton can be obtained by considering the even simpler case of flow above the equator. In this case,  $v$  and  $y$  are set to zero, and meridional derivatives are ignored. The result is a linear system of four equations for  $u', \theta', q', a'$ :

$$\frac{\partial u'}{\partial t} - \frac{\partial \theta'}{\partial x} = 0 \quad [32]$$

$$\frac{\partial \theta'}{\partial t} - \frac{\partial u'}{\partial x} = \bar{H} a' \quad [33]$$

$$\frac{\partial q'}{\partial t} + \tilde{Q} \frac{\partial u'}{\partial x} = -\bar{H} a' \quad [34]$$

$$\frac{\partial a'}{\partial t} = \Gamma \bar{a} q'. \quad [35]$$

This system can be solved exactly due to the perfect east–west symmetry:

$$2\omega^2 = \Gamma \bar{S}^\theta + k^2 \pm \sqrt{(\Gamma \bar{S}^\theta + k^2)^2 - 4\Gamma \bar{S}^\theta k^2 (1 - \tilde{Q})} \quad [36]$$

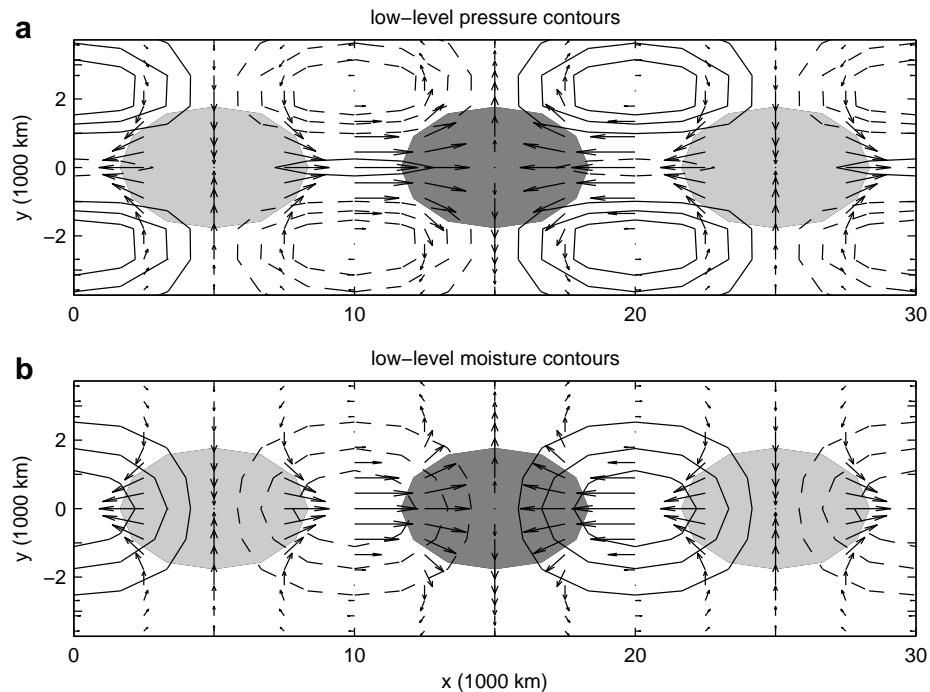


Figure 3: Physical structure of the wavenumber-2 MJO mode of [26]–[29] for the standard parameter values. Lower tropospheric velocity vectors are shown with contours of lower tropospheric pressure anomalies (a) and lower tropospheric moisture anomalies (b) with positive (negative) anomalies denoted by solid (dashed) lines. The contour interval is one-fourth the maximum amplitude of the anomaly, and the zero contour is not shown. Positive (negative) anomalies of convective activity  $A$  that are greater than one-half the maximum amplitude are shaded dark (light) gray. From Majda and Stechmann (2009) *Proceedings of the National Academy of Sciences USA*.

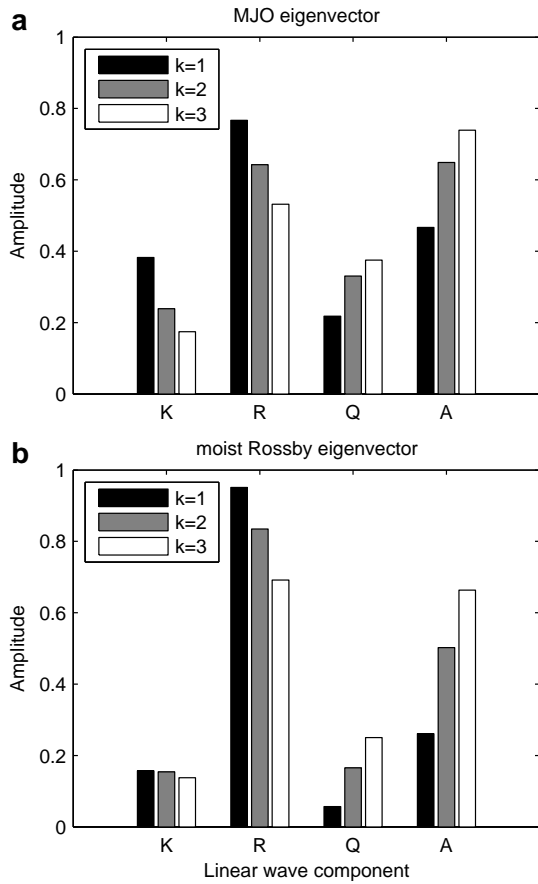


Figure 4: Contributions of each component  $K$ ,  $R$ ,  $Q$ , and  $A$  to the linear wave eigenvectors of the MJO (a) and the low-frequency westward-propagating mode (b) for the standard parameter values. Results for wavenumbers  $k = 1, 2$ , and  $3$  are shown in black, gray, and white, respectively. From Majda and Stechmann (2009) *Proceedings of the National Academy of Sciences USA*.

where  $k$  is the zonal wavenumber. For the low-frequency waves, this is approximately equal to

$$\omega \approx \sqrt{\Gamma S^{\bar{\theta}}(1 - \tilde{Q})}, \quad [37]$$

For the standard parameter values used here, the oscillation period corresponding to [37] is 45 days, in agreement with observations of the MJO. Notice that this formula is independent of the wavenumber  $k$ ; i.e., this model recovers the peculiar dispersion relation  $d\omega/dk \approx 0$  from the observational record, and it relates the MJO frequency to the three parameters of the model.

### 4.3 Nonlinear simulation

Figure 5 shows a numerical solution of the nonlinear equations [26]–[29] for a warm-pool sea surface temperature. The convective activity is aligned over the warm pool, which is in the center of the domain from  $x \approx 10,000 - 30,000$  km. The MJO events have prominent phases of both active and suppressed convection, and each event has its own individual characteristics in terms of strength, lifetime, regional variations, etc. Furthermore, in addition to the prominent eastward-propagating disturbances, there are instances of localized standing oscillations throughout the domain. For instance, to illustrate this, two rectangular boxes are drawn in Figure 5:  $x = 11,000 - 15,000$  km,  $t = 3,400 - 3,470$  days, and  $x = 15,000 - 19,000$  km,  $t = 3,440 - 3,530$  days. Localized standing oscillations are prominent again, later, in the region  $x = 15,000 - 19,000$  km,  $t = 3,550 - 3,600$  days (for comparison, no box added). The western end of the warm pool is a common location of the standing oscillations, which is in broad agreement with the visual appearance of standing oscillations in the Indian Ocean, sometimes at the beginning of an MJO event.

[FIGURE 5 ABOUT HERE]

## 5 MJO’s “muscle”

While the MJO skeleton model describes the fundamental planetary–intraseasonal features of MJO composites, individual MJO events often have additional features, such as westerly wind bursts, and different varieties of convective features within the MJO envelope. Since these additional features add detailed character to each MJO’s structure, and since these features often account for additional strength beyond the MJO’s skeleton, they are referred to here as the MJO’s “muscle.”

One contributor to the MJO’s muscle is convective momentum transport (CMT) due to the convective systems that are embedded within the MJO’s envelope. These systems include various types of MCSs and CCEWs, and their CMT can potentially accelerate or decelerate the winds associated with the MJO skeleton.

To illustrate the CMT due to MCSs and CCEWs, an exactly solvable model is presented for their velocity anomalies ( $u'$ ,  $w'$ ) and momentum fluxes  $\overline{u'w'}$  in a two-dimensional  $x - z$  setting above the equator. Consider the following exactly solvable model for a CCEW’s velocity ( $u'$ ,  $w'$ ):

$$w'(x, z, t) = S'_\theta(x, z, t) \quad [38]$$

$$\frac{\partial u'}{\partial x} + \frac{\partial w'}{\partial z} = 0. \quad [39]$$

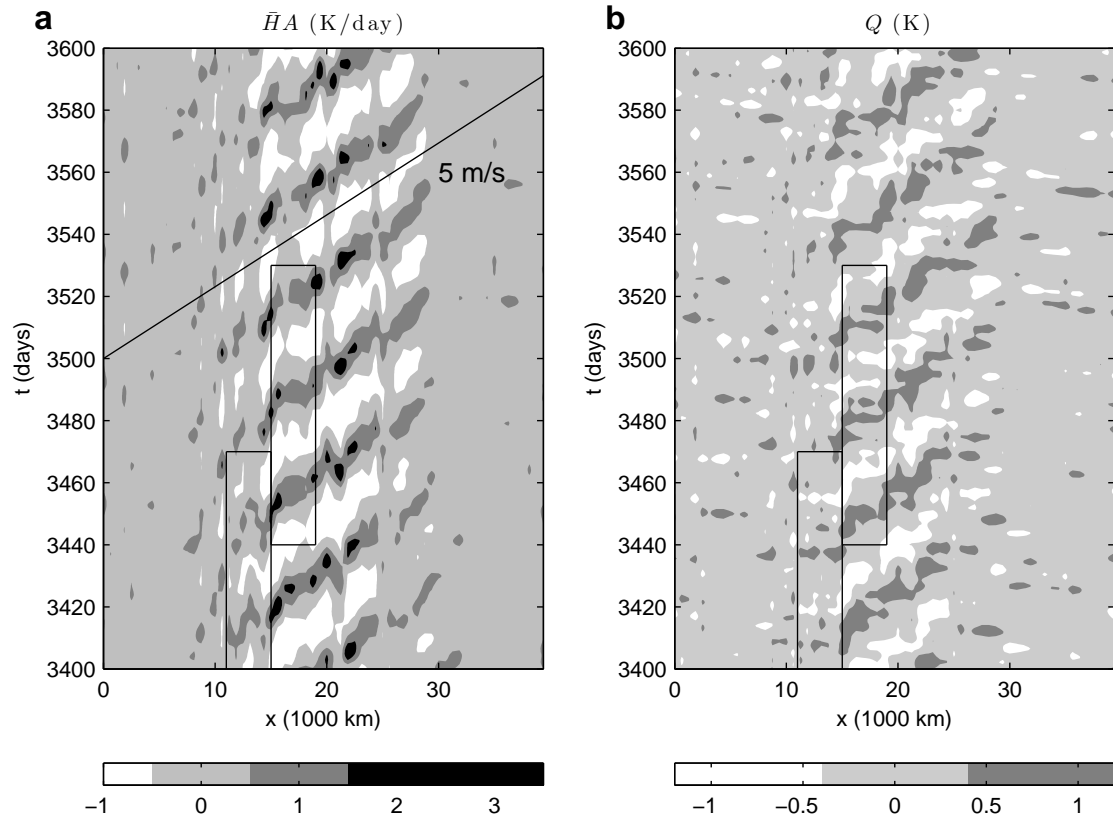


Figure 5: Numerical solution of the nonlinear equations [26]–[29] for a warm-pool sea surface temperature. Contour plots of (a)  $\bar{H}A'(x, t)$  and (b)  $Q'(x, t)$ . Rectangular boxes show regions of standing oscillations:  $x = 11,000$ – $15,000$  km,  $t = 3,400$ – $3,470$  days, and  $x = 15,000$ – $19,000$  km,  $t = 3,440$ – $3,530$  days. From Majda and Stechmann (2011) *Journal of the Atmospheric Sciences*.

In this model, called the weak-temperature-gradient approximation, the wave's vertical velocity  $w'$  is exactly in balance with the heating rate  $S'_\theta$ , which we must specify. The wave's horizontal velocity  $u'$  is then determined from the incompressibility constraint in [39]. Given this exact solution for  $u'$  and  $w'$  of the CCEW, its effect on the larger-scale mean flow is determined by

$$\frac{\partial \bar{u}}{\partial t} = -\frac{\partial}{\partial z} \overline{w'u'}, \quad [40]$$

where this is the horizontal spatial average of the horizontal momentum equation,  $\partial_t u + \partial_x(u^2) + \partial_z(wu) + \partial_x p = 0$ , and where bar and prime notation is used to denote a horizontal spatial average and fluctuation, respectively:

$$\bar{f}(z, t) = \frac{1}{L} \int_0^L f(x, z, t) dx \quad [41]$$

$$f'(x, z, t) = f - \bar{f}, \quad [42]$$

where periodic horizontal boundary conditions are assumed for simplicity. From [40] it is seen that a CCEW will alter the mean flow if and only if  $\partial_z \overline{w'u'} \neq 0$ . In the context of convective motions, this effect on the mean flow is called CMT.

To illustrate CMT in some specific cases, consider a heat source with two phase-lagged vertical modes,  $\sin(z)$  and  $\sin(2z)$ , which represent deep convective heating and congestus/stratiform heating, respectively:

$$S'_\theta = a_* \left\{ \cos[kx - \omega t] \sqrt{2} \sin(z) + \alpha \cos[k(x + x_0) - \omega t] \sqrt{2} \sin(2z) \right\}, \quad [43]$$

where  $k$  is the horizontal wavenumber and  $a_*$  is the amplitude of the heating. Two key parameters here are  $\alpha$ , the relative strength of the second baroclinic heating, and  $x_0$ , the lag between the heating in the two vertical modes. Heating structures of this form are commonly associated with MCSs and CCEWs, due to variations in congestus, deep, and stratiform cloud populations. Figure 6 shows three cases for the lag  $x_0$ : 0 (top), +500 km (middle), and -500 km (bottom) for a wave with wavelength 3000 km, heating amplitude  $a_* = 4$  K/day, and relative stratiform heating of  $\alpha = -1/4$ . The lag determines the vertical tilt of the heating profile. Given this heating rate, the velocity can be found exactly from [39]:

$$u'(x, z, t) = -\frac{a_*}{k} \left\{ \sin[kx - \omega t] \sqrt{2} \cos(z) + 2\alpha \sin[k(x + x_0) - \omega t] \sqrt{2} \cos(2z) \right\} \quad [44]$$

$$w'(x, z, t) = a_* \left\{ \cos[kx - \omega t] \sqrt{2} \sin(z) + \alpha \cos[k(x + x_0) - \omega t] \sqrt{2} \sin(2z) \right\} \quad [45]$$

With this form of  $u'$  and  $w'$ , the eddy flux divergence is

$$\frac{\partial}{\partial z} \overline{w'u'} = \frac{3 \sin(kx_0)}{2} \frac{a_*^2}{k} \alpha [\cos(z) - \cos(3z)] \quad [46]$$

Notice that a wave with first and second baroclinic components generates CMT that affects the first and *third* baroclinic modes. Also notice that [46] is nonzero as long as  $\alpha \neq 0$  (i.e., there are both first and second baroclinic mode contributions) and  $x_0 \neq 0$  (i.e., there is a phase lag between the first and second baroclinic modes). MCSs and CCEWs in nature typically have this type of structure.

For illustrations of the above exact solutions, consider the three cases shown in figure 6: upright updraft (top), “westward-propagating” CCEW (middle), and “eastward-propagating” CCEW (bottom). Although there is no inherent definitive propagation in the exactly solvable model [38]–[39], propagation direction labels are assigned to the vertical tilt directions according to the structures of observed CCEW: heating is vertically tilted with leading low-level heating and trailing upper-level heating with respect to the CCEW propagation direction. Specifically, Figure 6b corresponds to the observed structures of convectively coupled Kelvin waves, which propagate eastward, and Figure 6c corresponds to westward-propagating inertio-gravity waves (also called “two-day waves”). Also shown in Figure 6 are the average vertical flux of horizontal momentum,  $\overline{w'u'}$ , and its vertical derivative,  $\partial_z \overline{w'u'}$ . These exact solutions show that upright updrafts have zero CMT, and tilted updrafts have nonzero CMT with the sign determined by the CCEW’s propagation direction. Note that the vertically averaged momentum would not be affected by CMT in this model, since  $\overline{w'u'}$  is necessarily zero at the upper and lower rigid boundaries. Westerly wind bursts, which refer to lower tropospheric winds, can be accelerated by CMT due to eastward-propagating MCSs and CCEWs, as illustrated in Figure 6b.

[FIGURE 6 ABOUT HERE]

One effect that is not included in the model [38]–[39] is the effect of the larger-scale mean wind  $\bar{u}(z, t)$  on the MCSs or CCEWs. This could affect whether eastward- or westward-propagating convective systems are favored in a given environment, which, in turn, affects the CMT.

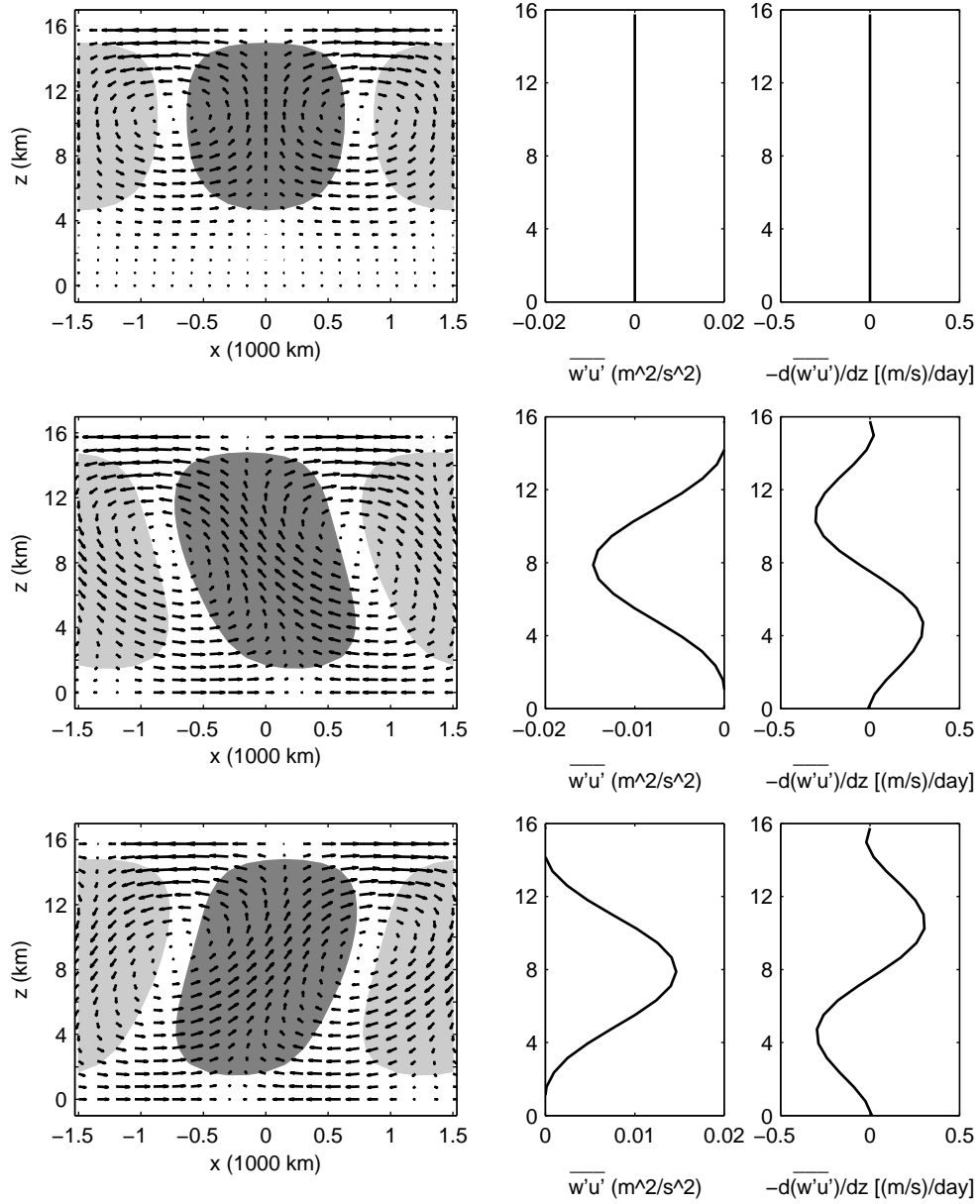


Figure 6: Solutions to the exactly solvable model [38]–[39] for CCEW structure and CMT in three cases: upright updraft (top), vertically tilted updraft of “eastward-propagating” CCEW (middle), and vertically tilted updraft of “westward-propagating” CCEW (bottom). Left: Vector plot of  $(u', w')$  and shaded convective heating  $S'_\theta(x, z)$ . For vectors, the maximum  $u'$  is 6.0 m/s for the top and 4.0 m/s for the middle and bottom, and the maximum  $w'$  is 2.8 cm/s for the top and 2.2 cm/s for the middle and bottom. Dark shading denotes heating, and light shading denotes cooling, with a contour drawn at one-fourth the max and min values. Middle: Vertical profile of the mean momentum flux:  $\overline{w'u'}$ . Right: Negative vertical derivative of the mean momentum flux:  $-\partial_z \overline{w'u'}$ . From Stechmann, Majda, and Skjorshammer (2012) *Theoretical and Computational Fluid Dynamics*.

## References

- Biello, J. A. and A. J. Majda, 2005: A new multiscale model for the Madden–Julian oscillation. *J. Atmos. Sci.*, **62**, 1694–1721.
- Khouider, B. and A. J. Majda, 2006: A simple multicloud parameterization for convectively coupled tropical waves. Part I: Linear analysis. *J. Atmos. Sci.*, **63**, 1308–1323.
- Kiladis, G. N., K. H. Straub, and P. T. Haertel, 2005: Zonal and vertical structure of the Madden–Julian oscillation. *J. Atmos. Sci.*, **62**, 2790–2809.
- Majda, A. J., 2003: *Introduction to PDEs and Waves for the Atmosphere and Ocean*, Courant Lecture Notes in Mathematics, Vol. 9. American Mathematical Society, Providence, x+234 pp.
- Majda, A. J. and S. N. Stechmann, 2009a: A simple dynamical model with features of convective momentum transport. *J. Atmos. Sci.*, **66**, 373–392.
- Majda, A. J. and S. N. Stechmann, 2009b: The skeleton of tropical intraseasonal oscillations. *Proc. Natl. Acad. Sci.*, **106** (21), 8417.
- Majda, A. J. and S. N. Stechmann, 2011: Nonlinear dynamics and regional variations in the MJO skeleton. *J. Atmos. Sci.*, **68**, 3053–3071.
- Moncrieff, M. W., 2010: The multiscale organization of moist convection and the intersection of weather and climate. *Climate Dynamics: Why Does Climate Vary?*, D.-Z. Sun and F. Bryan, Eds., American Geophysical Union, Washington, D. C., Geophysical Monograph Series, Vol. 189, 3–26.
- Tian, B., D. Waliser, E. Fetzer, B. Lambrigtsen, Y. Yung, and B. Wang, 2006: Vertical moist thermodynamic structure and spatial–temporal evolution of the MJO in AIRS observations. *J. Atmos. Sci.*, **63** (10), 2462–2485.
- Zhang, C., 2005: Madden–Julian Oscillation. *Reviews of Geophysics*, **43**, G2003+, doi:10.1029/2004RG000158.